Available online at www.sciencedirect.com

ScienceDirect

Journal of the European Ceramic Society 35 (2015) 1621–1635

www.elsevier.com/locate/jeurceramsoc

Chemical wear of Al_2O_3–MgO–C bricks by air and basic slag

Vanesa Muñoz [a], Pablo G. Galliano [b], Elena Brandaleze [c], Analía G. Tomba Martinez [a,*]

[a] INTEMA (CONICET), Av. Juan B. Justo 4302, 7600 Mar del Plata, Argentina
[b] Departamento de Tecnología de Refractarios – Tenaris REDE AR (CINI), Dr. Simini 250, 2804 Campana, Argentina
[c] Universidad Tecnológica Nacional, Colón 332, 2900 San Nicolás, Argentina

Received 3 August 2014; received in revised form 17 November 2014; accepted 20 November 2014
Available online 8 December 2014

Abstract

Al_2O_3–MgO–C (AMC) refractories are used in steelmaking vessels such as ladles, where they are part of the working lining's bottom and walls. Taking into account the conditions during the ladle operation, AMC refractories with high-melt corrosion resistance are required to provide good service performance. Moreover, due to the presence of graphite, AMC bricks should have low susceptibility to attack by oxidant gases. In this paper, the oxidation of commercial AMC refractories by air between 700 and 1400 °C and their corrosion by ladle basic slag at 1450 °C are examined. The experimental conditions for the chemical evaluation are similar to those to which AMC linings are exposed in some steps of the ladle operation. Differences in the chemical wear caused by both of the reagents among the studied bricks are associated to their differences in composition and microstructural and textural characteristics. In addition, the thermal evolution of each AMC refractory is considered.

Keywords: Al_2O_3–MgO–C refractories; Air oxidation; Basic slag corrosion

1. Introduction

The secondary refining ladle is no longer an inert vessel but rather a key piece, with multiple functions during the steelmaking process.[1] Tassot et al.[2] emphasize the importance of this vessel in current integrated metallurgical processes, to the point that the refractories composing it nowadays determine various aspects of both the process and the product.

Al_2O_3–MgO–C (AMC) refractory bricks are one of the materials used in the working linings of steelmaking ladles, being mostly used in the metal line and the bottom. Their application in the slag line is limited, due their susceptibility to basic melt attack at high temperature.[3] AMC bricks appeared in the '80 as an alternative to MgO–C and Al_2O_3–C refractories, and their main advantage is the reduction of joint wear due to controlled residual expansion by *in situ* spinel $MgAl_2O_4$ formation.[1,4–7] The scientific-technical literature on these types of materials has focused on this issue, at the expense of other aspects of refractory behaviour, mainly in comparisons with their antecessors, especially MgO–C bricks.

Depending on the logistics of the factory, the AMC refractories of the barrel and the bottom can be corroded by liquid slag, especially during tapping and casting. Since the ladle is an open vessel, AMC bricks are also exposed to attack by the gaseous atmosphere, to which they are susceptible due to the presence of graphite in their composition, in particular during casting and the periods of time when the ladle is empty, such as preheating and tapping in the continuous casting process. Melt corrosion and gases corrosion imply severe textual alterations and the loss of components that are critical to the AMC refractories' performance. For these reasons, resistance to chemical wear by liquid slag and oxidant gases is an aspect that has to be considered when improvements in the design and performance of these bricks are desired. In this sense, the more efficient and sure way to achieve these goals is to have basic information about the corrosion processes and the factors determining them, although these aspects have hardly been explored with regard to these types of refractories.[8,9]

In this context, this paper focused on the evaluation of the chemical wear on three commercial AMC bricks with

* Corresponding author. Tel.: +54 223 481600; fax: +54 223 4810046.
E-mail address: agtomba@fi.mdp.edu.ar (A.G. Tomba Martinez).

http://dx.doi.org/10.1016/j.jeurceramsoc.2014.11.024
0955-2219/

differences in MgO content and the source of corundum, due to the action of different chemical reagents in near-service conditions. Corrosion by atmospheric gases at temperatures between 700 °C and 1400 °C and the attack of basic slag at 1450 °C were examined. Analysis of the degradation caused by air was performed within a wide range of temperatures taking into account that the chemical and microstructural changes in oxide–C bricks begin at temperatures as low as 300 °C, particularly in the organic bonding.[10] Although this process will occur mainly in the first campaigns of the brick, the alterations to the composition and microstructure due to these reactions are severe. To analyze melt corrosion, a slag with a composition considered similar to that in contact with AMC refractories in service was used at a temperature that guarantees the fluidity of the slag. For experimental simplicity and in order to simulate the conditions existing at the end of casting, a cup test in air was used.

In contrast to the more widely employed practice for this type of study, which entails analyzing samples especially prepared in the laboratory and often pre-treated to pyrolize the organic binder, the commercial materials as used in plant were tested here. On one hand, the use of commercial bricks imposes limits with regard to controlling their composition, microstructure and texture, which thus requires their complete characterization in order to determine composition–microstructure/texture–behaviour relationships. On the other hand, this experimental strategy avoids the need to reproduce the fabrication process at a laboratory scale, which is not a trivial task, and the obtained information can be extrapolated directly into the steelshop.

2. Experimental procedure

2.1. Materials

Three Al_2O_3–MgO–C commercial refractory bricks manufactured by the same supplier and labelled as AMC1, AMC2 and AMC3 were analyzed. The bricks had differences in the MgO content and the type of raw material used as source of alumina.

Bearing in mind the aim of this work, these materials were exhaustively characterized using a vast group of analysis techniques, and the results have been previously reported by the authors[11]: X-ray fluorescence (XRF), plasma emission spectroscopy ((ICP-OES), gravimetry, X-ray diffraction (XRD), differential thermal and thermogravimetric analyses (DTA/TGA), reflection optical microscopy and scanning electron microscopy coupled with X-ray dispersive energy (SEM/EDS), measurements of density and porosity, Hg-intrusion porosimetry, dilatometric analysis and permanent linear change (PLC). The main refractories' characteristics are summarized in Table 1 and depicted below.[11]

Every refractory contains brown electrofused alumina (EF) plus tabular alumina (TA). AMC1 has a higher proportion of the last type of aggregates with respect to EF aggregates, and with respect to TA aggregates present in the other two materials as well. Furthermore, it was confirmed that only AMC3 possesses bauxite and that aluminium was added as antioxidant in the three materials, in similar proportions. The higher amount of sintered magnesia in AMC2 is distributed in the medium-fine fraction whereas this component is present in AMC1 and AMC3 only as fine particles in the matrix.

Graphite, whose particles have a similar aspect ratio in the three materials, is present at a higher content in AMC2, but its flakes are the smallest. The amount of graphite in AMC3 is somewhat lower and its particles are the purest. The bricks contain a similar amount of resin as organic binders.

Regarding the texture, AMC2 has a higher amount of open pores, although they are similar in size to those of AMC1. AMC3, however, is the brick with the lowest values of open porosity, permeability and pore size. The three AMC refractories have similar tortuosity parameters ~2 (determined by the Hg-intrusion porosimetry).

2.2. Oxidative degradation in air

The oxidative degradation of AMC refractories was evaluated in natural air (0.21 atm of O_2) in order to study the loss of components during the transformation of the resin and the direct oxidation of graphite. Thermal treatments in an airtight environment were carried out at 700, 1000, 1260 and 1400 °C, in duplicate, on cylindrical specimens 2.7 cm in diameter and 2.5 cm in height, which were cut from the original bricks. A chamber electrical furnace with SiC heating elements was used, with the following heating schedule: heating rate of 10 °C/min from room temperature (RT) up to the selected temperature, permanence of 2 h, and free cooling afterwards. The treated cylinders were packed in polyester resin in vaccum and cut crosswise. The cross surfaces were ground with SiC papers up to 4000 grit and diamond paste up to 3 μm, using kerosene as lubricant.

The mass loss and the decarburized superficial area, both in percentages, were determined as gaseous corrosion indicators. Images of the cross surface obtained with 4× magnification and the image analysis software Image-Pro Plus v.6 were employed to estimate the decarburized area of each sample, which was considered as that peripheral region in which a reduction of the black or dark colour was visually detected. A radius delimiting decarburized region from the central dark zone was defined, from which the decarburized area was calculated. The corrosion indicator was taken as the percentage of the total cross-area corresponding to the decarburized area of the specimen.

Moreover, mineralogical analysis by XRD in different areas identified on the cut surfaces – the dark inner zone (IZ) and the external or decarburized zone (OZ) – was performed. The analysis was carried out on a specimen's cross surface directly, using a Panalytical X'PERT PRO diffractometer, with Cu Kα radiation, 40 kV of voltage and a current of 40 mA. The measurements were done at a rate of 10°/min.

2.3. Basic slag corrosion

The chemical wear of AMC refractories by a typical ladle slag was studied at 1450 °C in air, employing the static cup test. Cubes 5 cm in length, with a whole 3.6–3.7 cm in diameter and 2.3–2.5 cm in height, into which the slag in powder was placed,

Table 1
Composition and texture data of AMC refractories.

		AMC1	AMC2	AMC3
Main phases	Corundum (Al_2O_3)	82.7 ± 0.3	57.6 ± 0.3	70.5 ± 0.3
(wt.%)	Periclase (MgO)	5.40 ± 0.02	27.0 ± 0.1	6.8 ± 0.1
Secondary phases	Mullite ($3Al_2O_3 \cdot 2SiO_2$)	–	–	8.6 ± 0.3
(wt.%)	Graphite (C)	1.7 ± 0.1	3.5 ± 0.1	3.0 ± 0.1
	Resin (C, O, H)	5.4 ± 0.1	5.6 ± 0.1	5.0 ± 0.1
	Aluminium (Al)	1.39 ± 0.02	1.37 ± 0.02	1.60 ± 0.02
Impurities (wt.%)	Fe_2O_3, SiO_2, CaO, TiO_2[a]	3.4 ± 0.3	4.9 ± 0.3	4.5 ± 0.3
Apparent porosity (%)		6.7 ± 0.1	7.8 ± 0.5	4.0 ± 0.1
Permeability (m^3/Nw/s)[b]		0.013	0.015	0.008
Minimum pore diameter (μm)		0.060	0.055	0.003

[a] Impurities expressed as oxides with contents >0.1 wt.%; others impurities are: K_2O, P_2O_5, Cr_2O_3, MnO, ZrO_2, SrO, ZnO.
[b] for ΔP of 3 MPa; ΔP is the pressure drop when the gas used in the measurement (N_2) passes through the sample.

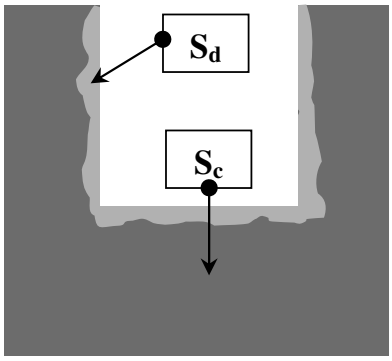

Fig. 1. Cross section of the corroded cup.

were used for the corrosion tests. These cups were thermally treated in a chamber electric furnace with SiC heating elements, at 1450 °C for 2 h. After the thermal treatments, the cups were packed in epoxy resin in vacuum. They were then cut transversally, and the cross surfaces were ground with SiC papers of 4000 grit and polished with diamond paste up to 3 μm, using kerosene as lubricant.

Corrosion was measured by the worn cross-area of the cup, which was a consequence of the irreversible loss of the refractory particles attacked by the slag. Photos were taken of the cross sections and the images were analyzed using Image Pro Plus 6.0 software. The new inner surface of the cup was delimited on the cross section image and used to calculate the worn area S_d as a percentage of the original cross-area of the cup, S_c (Fig. 1).

The slag used in the corrosion tests was that which was left in the ladle after the end of the continuous casting, and it was characterized by several experimental techniques. The slag was received from the plant in pieces and ground up to 70 μm using a planetary mill (Fritsch). This powder was quartered to obtain a representative sample, which was analyzed to determine its chemical and mineralogical compositions and its critical temperatures. The chemical analysis was performed by X-ray fluorescence using a Thermo Electron ARL model 9900. The mineralogical analysis was done by XRD using the same equipment and conditions mentioned above. Thermal differential and thermogravimetric analyses were carried out up to 1400 °C, in air, with a heating rate of 10 °C/min, with Shimadzu DTA-50 and Shimadzu TGA-50 thermal analyzers, respectively. To determine the critical temperatures of the slag (softening, hemisphere and fluidity temperatures), samples prepared with dextrin as a binder and a sintered alumina plate as a substrate were analyzed. The test was performed by hot stage optical microscopy using an equipment developed by our own laboratory (Metallurgy Department/DEYTEMA, UTN), with a heating rate of 5 °C/min up to 400 °C and then 10 °C/min up to 1500 °C. The basicity index of slag IB_2, defined as CaO/SiO_2 molar ratio, was calculated using chemical composition data. Moreover, the slag viscosity (η) between 1300 and 1600 °C was estimated using the Urbain model, which had been extensively used as a very good approximation of this property for steelmaking slags. The model assumes that every oxide in the slag affects the viscosity in the same way, depending only on its content.[12]

3. Results and discussion

3.1. Thermal evolution of AMC refractories

In previous work by the authors,[11,13] the thermal evolution of AMC1, AMC2 and AMC3 was studied by DTA/TGA up to 1400 °C in air and by isothermal treatments of refractory brick fragments at 700, 1000, 1100, 1200 and 1400 °C for 4 h, in airtight atmosphere.

For the three AMC materials, it was found[11] that the transformation of resin began at approximately 350–390 °C and the oxidation of residual glassy-carbon occurred at approximately 630 °C. Both reactions were accompanied by weight loss caused by the evolution of gases. Direct oxidation of graphite occurred in the range 900–990 °C, and there were evidences of a higher resistance to oxidation of graphite flakes present in AMC3, which was attributed to the higher purity of these particles.[11] When isothermal treatments of fragments of refractory bricks were done in air at 1000 °C during 4 h, it was determined by XRD that the three refractories lost their graphite completely.[13]

At temperatures >1000 °C, after the aluminium melting at ~660 °C, the reactions of this metal with the refractories' other components took place. They were accompanied by positive or negatives changes in mass in the three AMC materials.[11] The presence of Al_4C_3, formed by reaction of the aluminium with C coming from the resin pyrolisis or graphite, was confirmed

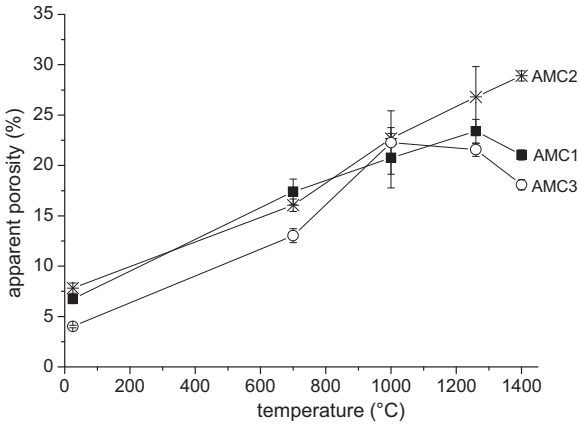

Fig. 2. Apparent porosity of AMC refractories as temperature increases (air atmosphere).

at temperatures between 1000 and 1200 °C. The formation of $MgAl_2O_4$ spinel was detected from 1100 °C onward, thus increasing the content of this phase as the temperature of the treatment increased.[13] It was inferred by the SEM/EDS analysis of some thermally treated samples that $MgAl_2O_4$ was formed by more than one reaction mechanism in each of the AMC refractories, *i.e.*, the combination of MgO with: (a) Al, (b) the products resulting from the reaction of the aluminium, such as Al_4C_3, and/or (c) alumina particles, including aggregates.

At 1400 °C, all the magnesia was consumed in AMC1 forming 21 wt.% of $MgAl_2O_4$ spinel, whereas MgO was still present in AMC2 and AMC3 at 1400 °C, and the amount of spinel was only 14 wt.% for both refractories.[11,13] These data indicate that spinel formed more easily in AMC1; this could be due to the higher proportion of fine and/or smaller sizes of alumina (possibly tabular alumina) and magnesia particles in this type of brick. Despite the fact that AMC3 has a nominal content of magnesia similar to AMC1, a rather smaller amount of spinel formed in the former. Moreover, since AMC2 contained a wide range of magnesia particle sizes (within fine, medium-size and coarse fractions), it could be possible that the proportion of the fine fraction, which is prone to react and form spinel, was lower than that present in AMC1 and AMC3.

In Fig. 2, the apparent porosity (π_a) of AMC1, AMC2 and AMC3 in air atmosphere is plotted as a function of temperature (these data were not previously reported). The dash-dot lines only join the media values for clarity.

The volumetric fraction of open pores grew gradually as the temperature increased up to 1000 °C. Resin transformation and direct graphite oxidation were the main sources of porosity in these AMC refractories and range of temperature. At the highest temperatures, the oxidation of impurities also contributed to porosity,[14] and the spinel formation could increase or reduce the amount of pores depending on the reaction mechanism.

AMC3, with lower initial apparent porosity and permeability, retained smaller open porosity volumes up to 1000 °C, when it reached those of AMC1 and AMC2. In contrast to those refractories, the difference among the apparent porosity of AMC3 specimens treated at 700 and 1000 °C was not considered significant. Between 1000 and 1260 °C, the volume of open pores remained almost unchanged for the three AMC refractories. At higher temperature, the porosity of AMC2 remained high, whereas AMC1 and AMC3 underwent a reduction of the volumetric fraction of open pores, more significant for the latter.

3.2. Oxidative degradation of AMC refractories in air

When AMC refractories are thermally treated in oxygen-enriched atmospheres such as air, this agent affects the pyrolisis of resin and oxidizes graphite. The analysis was centred on these two processes, dismissing the oxidation of impurities because they were minor components.

The pyrolisis of cured phenolic resins is thermally activated and consists of the scission of the hydrocarbon chain. It is a very complex process in which volatilization, condensation, oxidation, dehydration and decomposition reactions occur simultaneously.[15–17] The condensation and volatilization are accompanied by a loss in mass, volumetric shrinkage and porosity variation. The presence of oxygen in the atmosphere modifies the reaction mechanism and the composition of the scission products, and catalyzes the carbonization process.[16,17] The pyrolisis of phenolic resins ends with the formation of a condensed carboneous structure (carbonization) that is susceptible to oxidation, rigid, brittle, and non-graphitizable.

Direct oxidation of graphite takes place according to the following global reaction: $2C_{(s)} + O_{2(g)} \rightarrow 2CO_{(g)}$. Although there is not a general consensus regarding the exact steps which take place in direct graphite oxidation, some authors have proposed a general mechanism involving the reaction of flake edges, considered as the reactive sites, and the formation of ketonic superficial complex.[18,19]

The amount of C atoms removed from graphite surface by the action of oxygen and the proportion of CO and CO_2 (formed by the combination of the former with more O_2) depend on several factors.[20–23] According to that reported in literature regarding MgO–C refractories with and without metallic antioxidant additives, direct oxidation of graphite at high temperatures (>800 °C) is controlled by oxygen diffusion.[24–26] At a fixed temperature, gas diffusion is strongly affected by: (a) the gradient of O_2 partial pressure between the surface and interior of the material, (b) the open porosity, permeability and pore size of the refractory, (c) the evolution of these properties in the more external layers of the specimen and (d) the counter-diffusion of reaction products.

Images of the cross surfaces of specimens treated in air in the range 700–1400 °C are shown in Fig. 3, together with images of the original AMC bricks. Percentages of decarburized area and mass loss as the treatment temperature increases are plotted in Figs. 4 and 5, respectively.

According to thermal evolution of AMC materials (Section 1), oxidative pyrolisis of resin was expected to have occurred at least partially at 700 °C, and the direct oxidation of graphite could also begin. Resin pyrolisis as a thermally activated process will take place throughout the entire specimen. However, the catalytic effect of O_2 will produce a gradient in the advance of the transformation as the gas penetrates the material. Meanwhile, direct oxidation of graphite will occur mainly in the outer layers in contact with oxygen and spread towards the interior of the

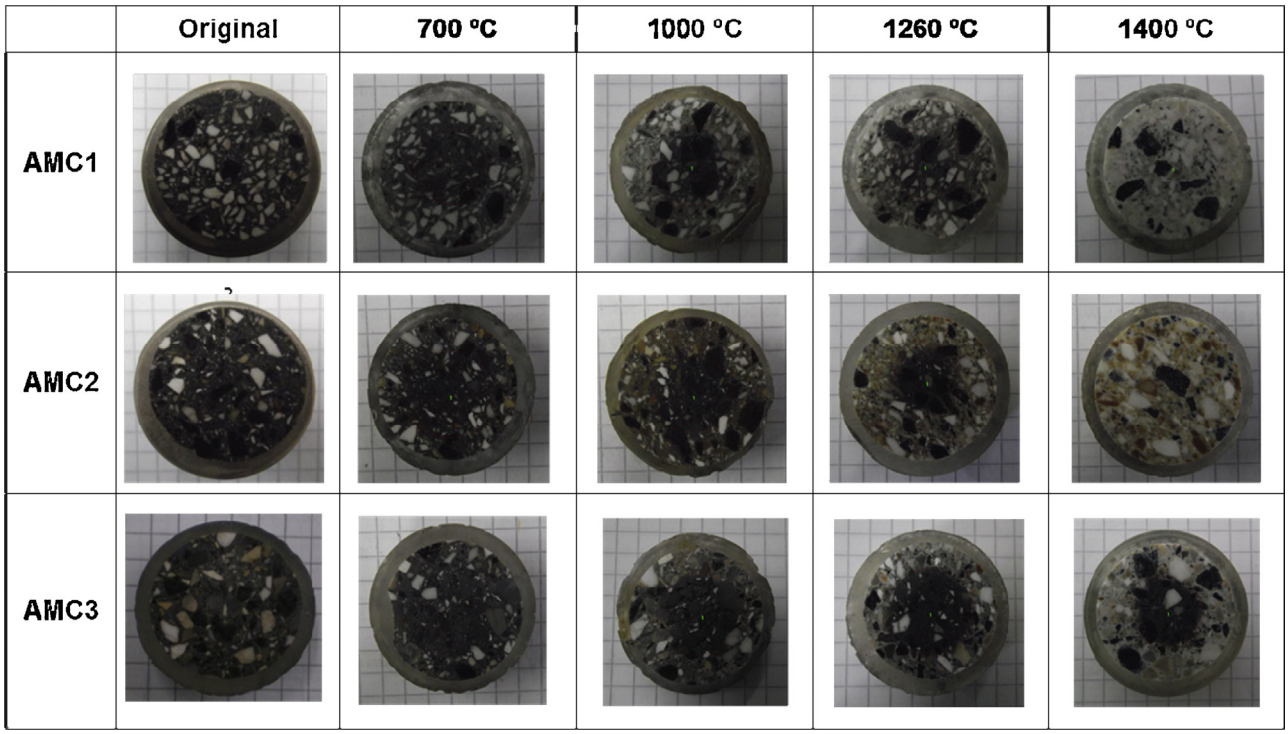

Fig. 3. Cross surface images of AMC refractories thermally treated in air.

specimen as the O_2 of air enters through the open pores towards, giving the typical patterns observed in most of the cross surfaces of Fig. 3.

In AMC1 and AMC2 refractories treated at 700 °C, the decarburized peripheral zone with a reaction front delimiting a darker centre and a superficial zone was observed. The decarburized layer corresponded to 60–70% of the total cross area. The weight losses, 5.8 wt.% in AMC1 and 6.5 wt.% in AMC2 were higher than the respective content of resin (AMC1: 5.4 wt.%; AMC2: 5.6 wt.%) which confirmed the fact that both refractories lost graphite by direct oxidation at 700 °C.

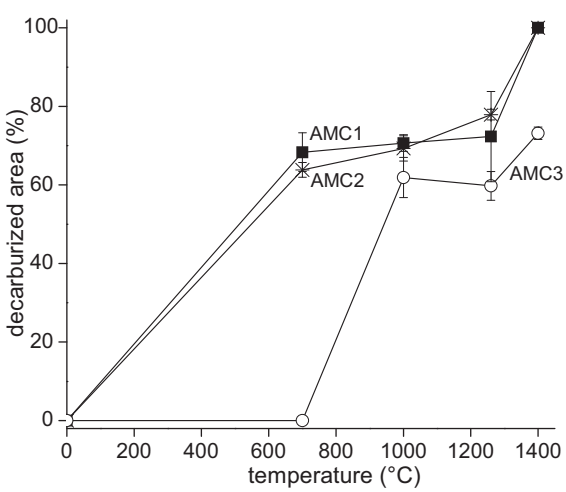

Fig. 4. Percentage of decarburized area of AMC refractories as a function of the treatment temperature (the dash-dot lines only join the media values for clarity).

Conversely, no discoloration was observed on the surfaces of AMC3 specimens treated at 700 °C. Even so, a loss in mass of 4.7 wt.% (Fig. 5) was determined due to the oxidative pyrolisis of resin that was not completely lost (organic binder content in the original material was 5.0 wt.%). These facts can be taken as indication of a lesser advance of the oxidative pyrolisis of resin and a delay in the onset of the graphite oxidation in comparison with the other two AMC bricks. The differences in the behaviour of AMC3 with respect to the other two AMC materials treated at 700 °C were attributed to its lower volume of open porosity in this temperature range (Fig. 2), which reduces the amount of O_2 able to penetrate into the specimen from the outer surface. Moreover, it is expected that the permeability and the mean pore size, which were smallest in the original AMC3 brick, also retained their low values at 700 °C. Doughty and Tovey[23] have reported that graphite flakes exhibit lower oxidation resistance the higher content of impurities they have, because the impurities provide a more efficient means to penetrate into the micropores present in the particles favouring their oxidation. For this reason, the higher oxidation resistance of the purer graphite flakes of AMC3[11] could also contribute to delay graphite oxidation.

At temperatures <900 °C, the direct oxidation of graphite is controlled by the diffusion of the gas through the pores of the flakes.[22] According with the results obtained after the treatment of AMC materials at 700 °C and previously reported data about oxidation of other carbon-containing bricks,[10,24–26] it was inferred that the diffusion of O_2 was meanwhile determined by the transport of the gaseous specie trough the pores of the refractory.

After treatment at 1000 °C, the external part of the cross surface in each material underwent more pronounced

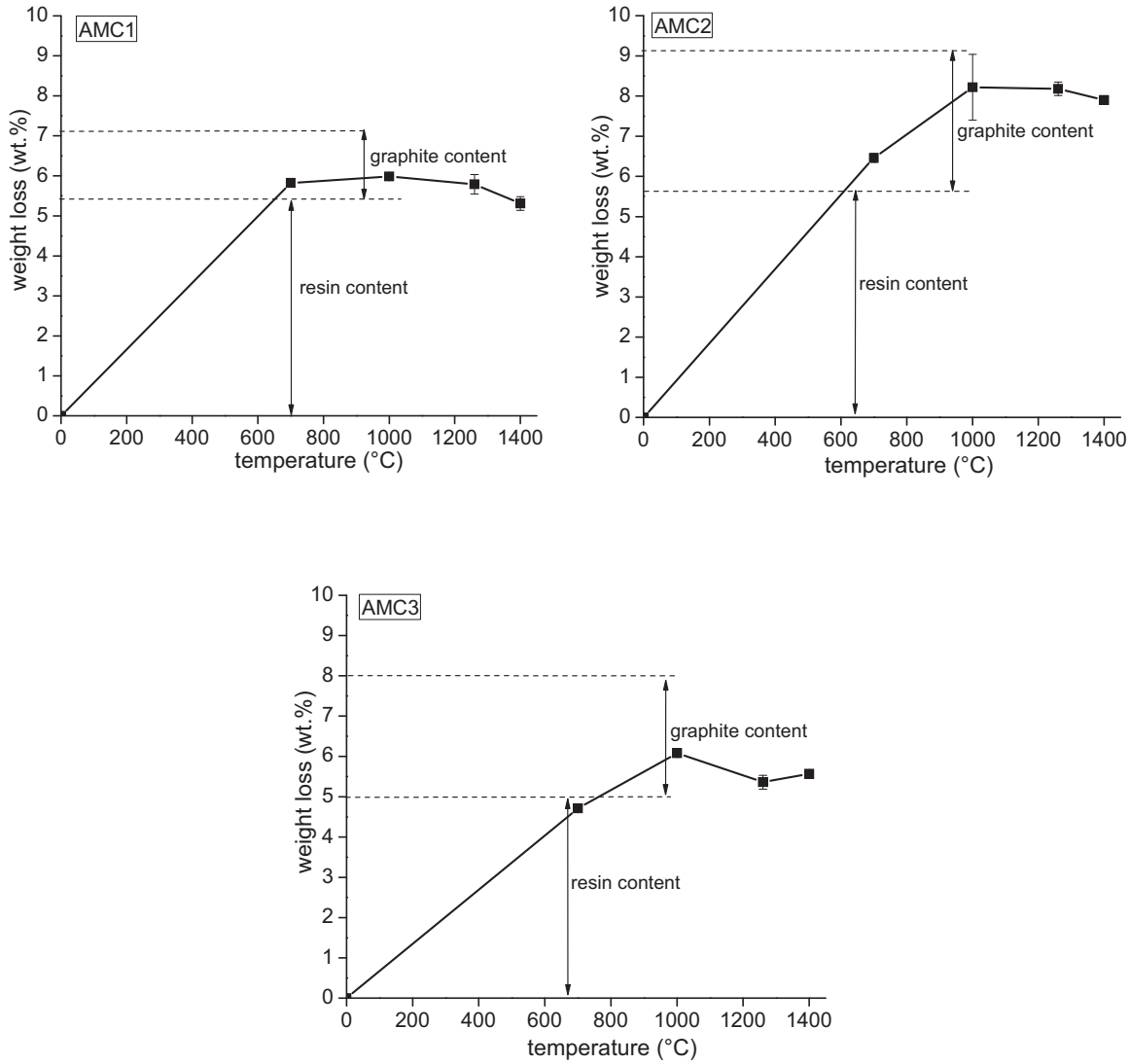

Fig. 5. Percentage of weight loss of each AMC refractory, as a function of treatment temperature (dashed line: resin and graphite contents; full lines only join the media values for clarity).

decarburization in comparison with treatment at 700 °C (Fig. 3), suggesting that a greater amount of graphite loss took place in this condition. Despite this, the percentage of the decarburized area was almost the same in AMC1 with respect to the value determined for this indicator after thermal treatment at 700 °C; this was also true for the weight change. The lack of change in the advance of the reaction front could be attributed to several effects. Although the direct graphite oxidation reaction is controlled by the limit layer at this temperature,[22] this process is still determined by the diffusion of O_2 through the material's pores in the case of carbon-containing refractories. Pötschke et al.[27] proposed an analytical expression (Eq. (1)) for the advance of the reaction front into the specimen (x) with time (t) at a fixed temperature (T):

$$\frac{dx}{dt} = -2V_G D_p \frac{n_0 - n_i}{x_0 - x} \quad (1)$$

where V_G is the molar volume of graphite, D_p is the diffusion coefficient of oxygen in the decarburized area, n_0 and n_i correspond to O_2 concentration in air and at the reaction front, respectively, and x_0 is the radius of the specimen. Furthermore, D_p is expressed as (Eq. (2)):

$$D_p = D\varepsilon\gamma \quad (2)$$

with D being the diffusion coefficient of the gas at T, ε the open porosity volume fraction (*i.e.*, $\varepsilon = \pi_a/100$, where π_a is the apparent porosity) and γ a labyrinthine factor that could be related inversely with the tortuosity of the pores.[28] Taking into consideration these mathematical expressions, it is clear that the reaction front advances more as the porosity of the decarburized layer and the difference of the oxygen concentration between the external atmosphere and specimen's interior increase.

The direct oxidation of graphite leads to an increase in open porosity, which is more significant in the outer layers of the specimen. The porosity change is complex since the graphite loss creates slit pores with dimensions similar to those of the flakes.[28] This also increases the connectivity and the tortuosity

of pores, thus changing the permeability, which in turn affects the O_2 diffusion.

On the other hand, it has been reported that some of the sub-products of the reaction, such as soot (formed by: $2\,CO_{(g)} \rightarrow CO_{2(g)} + C_{(s)}$), could block pores.[26] Moreover, resin transformation in this range of temperatures leads to the closure of open micropores (even though it was a source of open pores and fissures before).[15] These last two processes reduce the access channels for O_2 and could decrease the D_p coefficient, thus producing an accumulation of gas, with both factors tending to lower the advance of the reaction front. In contrast to what happened with the other two refractories, AMC1 did not show a significant increase in open porosity between 700 and 1000 °C, as can be observed in Fig. 2, which could be a consequence of the mentioned effects. Another process that could partially inhibit the entrance of O_2 is the counter-diffusion of the gaseous reaction products.

The formation of soot could also compensate for weight loss due to graphite oxidation contributing, at least in part, to the deceleration of this indicator in AMC1 between treatments at 700 and 1000 °C (Fig. 5). Another cause for this behaviour may be the beginning of the combination reactions of Al with other refractory components such as carbon (Section 1), some of which are associated with weight increase.[11]

In the AMC2 refractory treated at 1000 °C, there was greater decarburization of the peripheral zone in comparison with treatment at 700 °C, along with an advance of the reaction front and greater weight loss, which was consistent with a higher amount of direct graphite oxidation. The behaviour of AMC2 was also consistent with the apparent porosity increase (Fig. 2), which could facilitate the entry of oxygen into the material, the occurrence of the oxidative degradation reactions and an increased amount of graphite loss, as inferred from the plot of Fig. 5. The smaller size of the graphite flakes present in AMC2[11] favoured their oxidation, according to that reported by Doughty and Tovey.[23] In contrast to what could happen in AMC1, it is probably those factors mentioned previously that lead to a net increase in the open porosity in the outer zone of the cylinder, increasing D_p and x in Eq. (1), would dominate the process in AMC2. Even though the initial tortuosity was similar in the three AMC refractories (~2), an effect caused by this parameter cannot be ruled out since tortuosity was expected to change differently in each of the materials with temperature due to the resin and graphite reactions.

After treatment at 1000 °C, the AMC3 refractory exhibited discoloration on the outer surface that almost attained the value of this indicator in the other materials, both of which were very similar (~70%, Fig. 3). This variation was accompanied by a percentage of weight loss higher than that determined at 700 °C and similar to that of AMC1 (~6 wt.%). This behaviour was consistent with the remarkable increase in the volumetric fraction of open pores observed in AMC3 between 700 and 1000 °C (Fig. 2). Since the graphite flakes of AMC3 seem to be more resistant than these type of particles in the other two materials, the proportion of graphite consumed during the treatment at 1000 °C was relatively low (<50 wt.% according Fig. 5).

The degree of decarburization continued to increase after treatments at 1260 °C in air, and there was still a darker central zone in each material. AMC1 displayed behaviour similar to that observed at 1000 °C, which confirmed the factors that were involved; these factors were principally the compensation of the loss in mass due to graphite oxidation, with the increase in mass related to the reactions involving aluminium and, in this range of temperature, spinel formation. This new phase was identified in X-ray diffractograms in both regions of the cylinders, in the inner and outer regions. In AMC2, the oxidation reaction front continued to advance, in agreement with the increase in apparent porosity, but weight loss remains unchanged, product of the reactions involving the antioxidant and magnesia. In comparison with AMC1, the formation of new solid phases manifested itself at higher temperature, as was determined in the thermal evolution of these materials (Section 1).

Between treatments at 1000 and 1260 °C, AMC3 exhibited changes similar to those observed between 700 and 1000 °C: higher discoloration, mainly in the peripheral region, with no significant change in the percentage of the decarburized area. This last fact can be justified by the same causes discussed above (reduction of the open pores due to the closure of micropores, soot deposition and/or the counter-diffusion of gaseous products), taking into account that the temperature corresponding to the onset of the oxidative process was observed to be higher in AMC3 with respect to the other two refractories.[11] Fig. 2 shows that the apparent porosity was indeed unchanged in AMC3 between 1000 and 1260 °C. Weight loss was even lower after the treatment at 1260 °C, which indicated that the reaction involving Al compensated for the graphite loss.

Finally, surfaces of AMC1 and AMC2 specimens treated at 1400 °C were completely decarburized (Fig. 3), whereas AMC3 showed a dark centre, indicating that graphite was still present in this condition. In AMC2 and AMC1, the loss of graphite was counterbalanced by the formation of new phases, to a higher degree in AMC1 as was discussed above. A significant reduction in the volume of open pores was also observed in AMC1 between 1260 and 1400 °C (Fig. 2). Conversely, the graphite loss at 1400 °C, which was hindered due to the significant decrease in the apparent porosity, was more significant than the mass gain as consequence of the formation of new solid phases in AMC3.

The qualitative variations in the more intense peak of graphite (26.38° 2θ; File ICDD 41-1487) displayed in X-ray diffractograms of inner (IZ) and outer (OZ) zones, in comparison with the original material are reported in Table 2. The change of the amount of 'x' with treatment temperature is an estimation of the change of the intensity of the main XRD graphite peak in each AMC refractory. The differences in the initial content of graphite between AMC materials in Table 2 were dismissed.

The reduction in the intensity of the main X-ray diffraction peak of graphite diffraction peak was consistent with the extent of decarburization in a major part of cases. However, there were some exceptions, such as the case of AMC2 treated at 700 and 1000 °C which showed an unexpected increase in the intensity of the peak around 26.4° 2θ (Table 2). The reason for this disturbance was found in the contribution of residual carbon produced by resin pyrolisis, which diffracts similarly to graphite.[29] It was

Table 2
Variation in the intensity of the main XRD peak of graphite (26.38° 2θ) with the treatment temperature (IZ: inner zone; OZ: outer zone).

		AMC1	AMC2	AMC3
As-received[a]		xxxxx	xxxxx	xxxxx
Treatment temperature				
700 °C	IZ	x	xxx	xxxxx
	OZ	xx	x	xxxxxx
1000 °C	IZ	xx	xxxxx	xxxx
	OZ	xx	xxxx	xxxx
1260 °C	IZ	xxx	xxx	xxxx
	OZ	x	x	xx
1400 °C	IZ	–	–	x
	OZ	–	–	–

[a] Differences in the graphite content of the original AMC bricks have been dismissed.

considered that the greater amount of open pores in AMC2 promoted the entrance of O_2 and thus the transformation of resin (which seems to be complete at this temperature as Fig. 5 shows). In the case of AMC3 treated at 700 °C, the main peak of graphite was even greater in OZ than in the original material due to the contribution of residual carbon plus the graphite that was not oxidized yet. At 1400 °C, the absence of graphite diffraction peaks in the different zones of AMC1 and AMC2 was in agreement with the observation of complete decarburization. Conversely, a low intensity peak around 26.4°2θ was identified in the inner zone of AMC3, in accordance with the permanence of the dark centre in the treated specimen (Fig. 3).Bearing in mind the information collected from thermal treatments in air between 700 and 1400 °C, it was established that AMC3 was the most resistant of the three refractory materials to air corrosion due to its low apparent porosity that, except at 1000 °C, maintained smaller values than AMC1 and AMC2, and higher inherent oxidation resistance of its own graphite flakes. At the other extreme, AMC2 was the refractory showing the lowest oxidation resistance in air. As the temperature of the thermal treatments increased, the percentage of decarburization continually increased in this material, which was consistent with the overall increase in its open porosity values and the content and size of its graphite flakes. In this way, the main compositional differences between the studied AMC refractories (MgO content and type of alumina source) had an indirect influence on their susceptibility to oxygen through their effect on packing and, in consequence, on the open porosity and the degree of interconnection (permeability). In this sense, their granulometric distribution in the coarse fraction as well as in the medium-sized and fine fractions had an influence greater than that of the chemical nature of the raw materials.

3.3. Basic slag corrosion of AMC refractories

In the case of steelmaking ladles where AMC bricks are used, the liquid slag present during the secondary refinement of steel is a powerful corrosive agent due to its chemical incompatibility with the composition of the refractory lining.[30] The basic nature of slag (high CaO/SiO_2 molar ratio) makes it efficient in picking up of the sub-product of the process. Nevertheless, these slags have significant variations in the content of other components

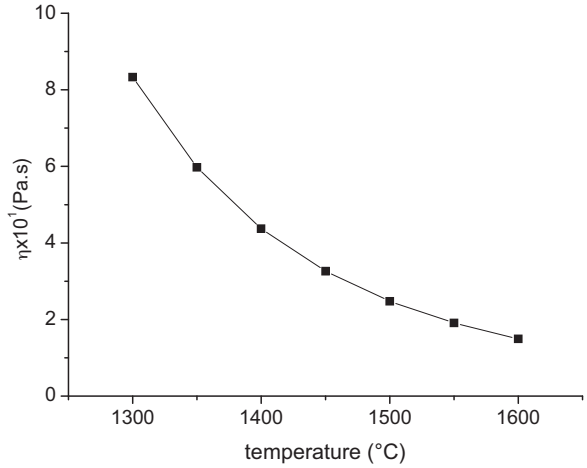

Fig. 6. Slag viscosity in function of temperature.

such as Al_2O_3, for instance; in general, ladle slags at the end of the process are Al_2O_3-rich.[31]

The corrosion of the main oxidic components of AMC refractories, *i.e.*, alumina, magnesia and $MgO{\cdot}Al_2O_3$ spinel formed at $T > 1000$ °C has been extensively treated in model systems.[30,32] The phases which are usually formed as products of reactions with CaO-, Al_2O_3-, MgO- and SiO_2-containing slags are well-known. The information obtained from tests of simple model systems of one-phase particles is useful to interpret the corrosion of high complexity refractories such as those containing carbon, which also have ceramic, metallic and organic raw materials. However, it is just a good starting point and other determining factors such as the effect of the material's texture and the effects caused by the atmosphere, the type of antioxidant additives and the organic binders in systems bonded with C have to be also considered.[32]

3.4. Slag characterization

Data of slag chemical analysis determined by XRF are reported in Table 3. The basicity index IB_2 was 10.8, indicating its basic character.

The presence of sulphur was due to the refinement process that took place in the ladle and, as the high content of Al_2O_3,[31] the origin of the used slag. From the data of Table 3, the evolution of slag viscosity (η) with temperature between 1300 and 1600 °C was estimated (Fig. 6).

The X-ray diffractogram of the slag (crystallized during cooling) is shown in Fig. 7. The presence of mayenite ($12CaO{\cdot}7Al_2O_3$), anorthite ($CaO{\cdot}Al_2O_3{\cdot}2SiO_2$), dicalcium aluminate ($CaO{\cdot}2Al_2O_3$), periclase (MgO), spinel ($MgO{\cdot}Al_2O_3$), lime (CaO), sulphur (S), brucite ($Mg(OH)_2$) and tricalcium aluminate ($3CaO{\cdot}Al_2O_3$) was confirmed. These are phases commonly present when the steelmaking ladle slags crystallized during the cooling.[33,34]

The softening, hemisphere and fluidity temperatures for the slag were: 1366 ± 5 °C, 1385 ± 5 °C and 1393 ± 5 °C, respectively. These values were consistent with the fluidity of the system inferred by DTA thermogram (Fig. 8). From this

Table 3
Chemical analysis of slag (XRF).

	SiO_2	CaO	Al_2O_3	MgO	FeO	MnO	Cr_2O_3	S
wt.%	5.040 ± 0.100	54.94 ± 0.600	30.833 ± 0.700	8.187 ± 0.290	0.374 ± 0.040	0.120 ± 0.002	0.015 ± 0.002	0.517 ± 0.006

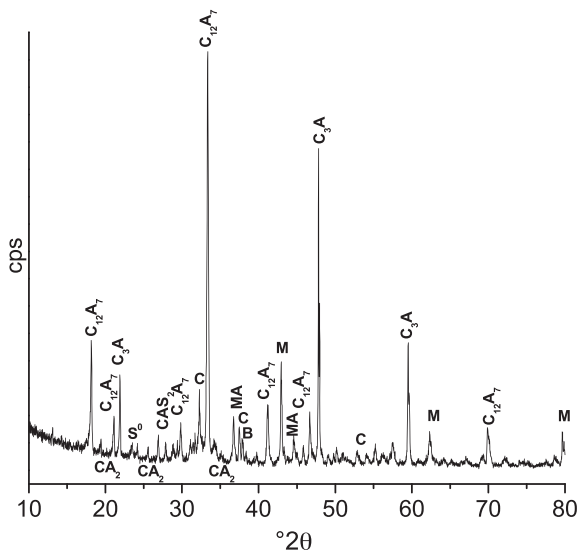

Fig. 7. X-ray diffractogram of slag. ($C_{12}A_7 = 12CaO{\cdot}7Al_2O_3$, $CAS_2 = CaO{\cdot}Al_2O_3{\cdot}2SiO_2$, $CA_2 = CaO{\cdot}2Al_2O_3$, $C_3A = 3CaO{\cdot}Al_2O_3$, M = MgO, $MA = MgO{\cdot}Al_2O_3$, C = CaO, $B = Mg(OH)_2$, S^0 = sulphur.)

information, it was considered that temperatures higher than 1400 °C guarantee that slag has high fluidity. At the slag fluidity temperature (1393 °C), the estimated viscosity was 0.45 Pa s (Fig. 6), whereas at 1450 °C, which was the temperature selected for the corrosion test, it fell down to 0.32 Pa s.

3.5. Corrosion test

Cross section images of each refractory cup are shown in Fig. 9, from which the wear was calculated as the percentage of corroded area: 5, 12 and 9% for AMC1, AMC2 and AMC3, respectively. The presence of remnant slag was observed, in a greater amount for materials AMC1 and AMC3, as well as the superficial oxidation of the cups by the atmospheric oxygen that overlapped to the slag corrosion.

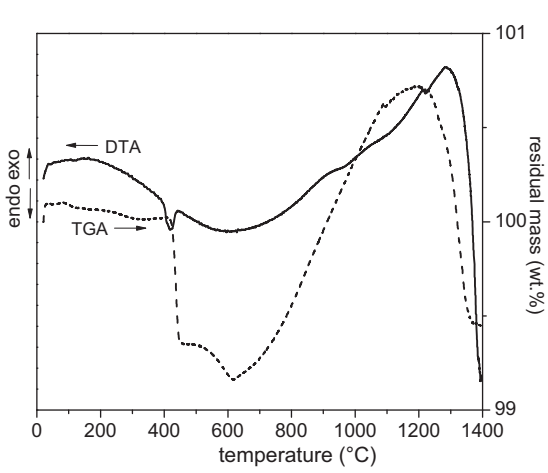

Fig. 8. DTA and TGA thermograms of the slag.

The aspect of cups after corrosion tests suggested that the material more susceptible to the attack of the tested basic slag was AMC2, which showed extensive slag penetration and wear; it was followed by AMC3, which exhibited less wear and very low slag penetration. AMC1 at the end, showed a higher resistance to slag corrosion (little penetration and low percentage of corroded area).

The analysis of refractory–slag interfaces by SEM/EDS was carried out looking at the reacted matrix and the different kind of aggregates present in each material. A high deterioration of the bonding phase was observed in every AMC material, manifested in the presence of the resin used to pack the specimen in this region, due not only to the slag corrosion but also the processes taking place within the material at high temperature (resin pyrolisis and graphite oxidation, in principle). The state of the matrix at the interface with the slag prevented the analysis of the presence or absence of graphite in this region by SEM/EDS as well as the *in situ* $MgAl_2O_4$ spinel.

SEM images of the tabular alumina aggregates of AMC1, AMC2 and AMC3, together with the phases identified by EDS (dotted lines indicate the refractory–slag interface) are shown in Fig. 10. The analysis of the particles pointed out the presence of elements such as Mg and S, absent in the original state of the bricks, and an increase in Na content, which suggested the penetration of the melt into this type of aggregates. Since the slag did not contain an appreciable amount of sodium, the amount of this element was attributed mainly to the dissolution of the fine tabular alumina particles of the matrix, which have $Na_2O{\cdot}11Al_2O_3$ (β-alumina) as typical impurity.

In general, calcium aluminates were identified as has been reported in the literature when alumina is attacked by $CaO–MgO–Al_2O_3–SiO_2$ slags. The formation of successive layers of these phases, each one with different composition, was observed around the aggregates (indirect corrosion[30]), although the boundaries between layers were diffuse, even more so in AMC2 and AMC3. Calcium hexaluminate (CA_6) formed a very thin continuous layer next to the aggregate. This phase was the product of the reaction of alumina, whose concentration had been increased locally due to the dissolution of the particle in the melt, with the CaO present in the slag. The presence of this layer is beneficial if it behaves as a physical barrier, protecting the refractory from a further attack on the slag and provided that it is continuous and thick.[35] The reduced thickness of the layer around the tabular alumina aggregates questioned the protective role of CA_6 in these cases.

As the distance from the alumina aggregate to the slag and Ca content increased, CA_2 with low proportion of Al_2O_3 was preferably formed, and CA later. It is possible that the formation

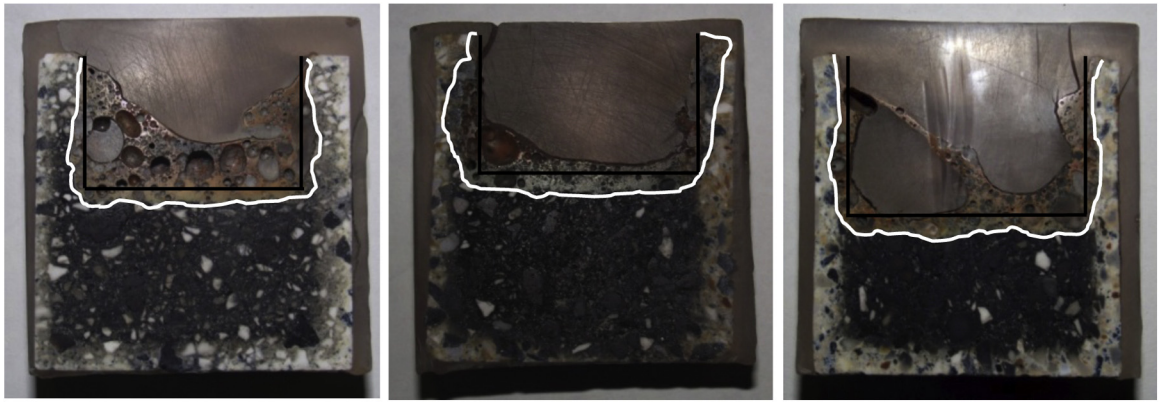

Fig. 9. Cross surfaces of AMC cups treated at 1450 °C. (black line: original hole's surface; white line: hole's surface after slag attack).

of CA_2 preceded the CA_6 phase[35] due to the latter's reaction with the Al_2O_3 from the melt or the solid aggregate. Apparently, CA_2 also constituted a continuous layer surrounding CA_6. Phases with even lower proportions of Al_2O_3, such as C_3A or $C_{12}A_7$, were identified within the slag, which could correspond to components of the original slag crystallized during cooling.

On the other hand, the interaction between tabular alumina aggregates of AMC refractories and the basic slag led to spinel $MgAl_2O_4$ (MA) formation, which was detected near the tabular alumina particle, as has been reported by other authors.[36] The presence of spinel favours corrosion resistance by the dissolution of ions, mainly those of iron. However, the effectiveness of the corrosion protection by the indirect corrosion mechanism is partially linked to the fact the new phase forms a continuous layer in front of the solid particle. The MA layer was continuous in AMC1, as can be observed in Fig. 10, but spinel was present as an isolated particle or cluster of particles in AMC2 and AMC3. This difference in the feature of spinel when corundum particles are attacked by CMAS slag has been attributed to differences in the MgO concentration in the melt.[36] The amount and size of these spinel clusters seemed greater in AMC2 than in AMC3, attuned to its higher content of MgO, which could be dissolved in the liquid.

Moreover, ternary phases containing SiO_2 were identified in the vicinity of the tabular alumina aggregates of AMC3 and AMC2; this included gehlenite (C_2AS) and anorthite (CAS_2), respectively. These ternary phases are responsible for the appearance of liquid at temperatures near 1250 °C.[8] Meanwhile, the

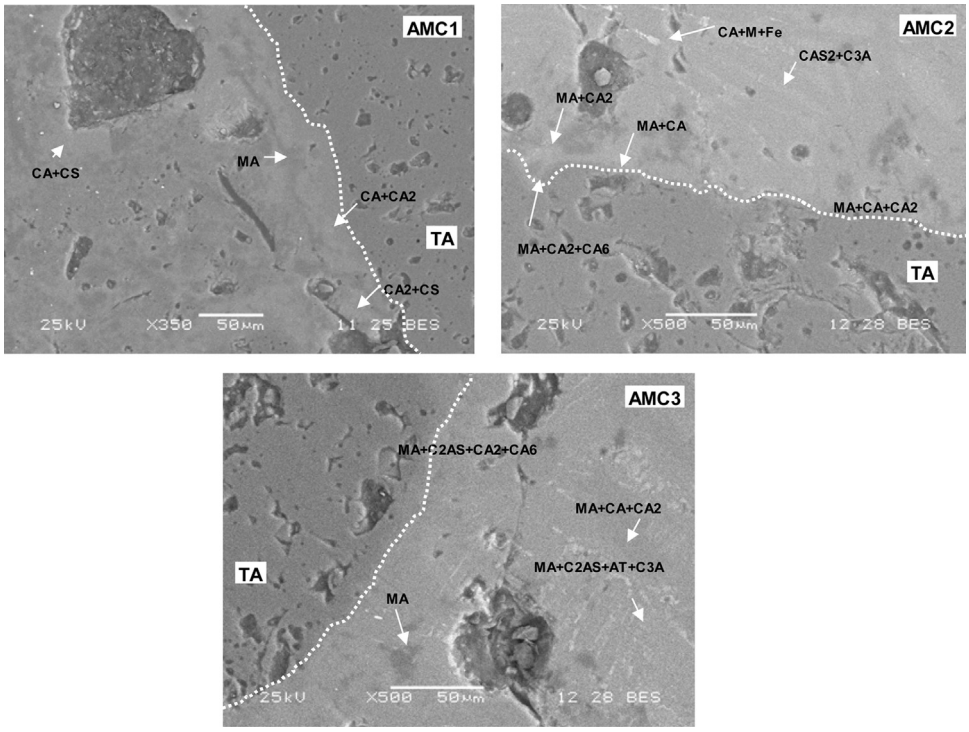

Fig. 10. Tabular alumina particles (TA) corroded by the slag. ($C_3A = 3CaO{\cdot}Al_2O_3$, $CA = CaO{\cdot}Al_2O_3$, $CA_2 = CaO{\cdot}2Al_2O_3$, $CA_6 = CaO{\cdot}6Al_2O_3$, $CS = CaO{\cdot}SiO_2$, $C_2AS = 2CaO{\cdot}SiO_2{\cdot}Al_2O_3$, $CAS_2 = CaO{\cdot}Al_2O_3{\cdot}2\,SiO_2$, M = MgO, $MA = MgO{\cdot}Al_2O_3$, $AT = Al_2O_3{\cdot}TiO_2$, $Fe = Fe^0$.)

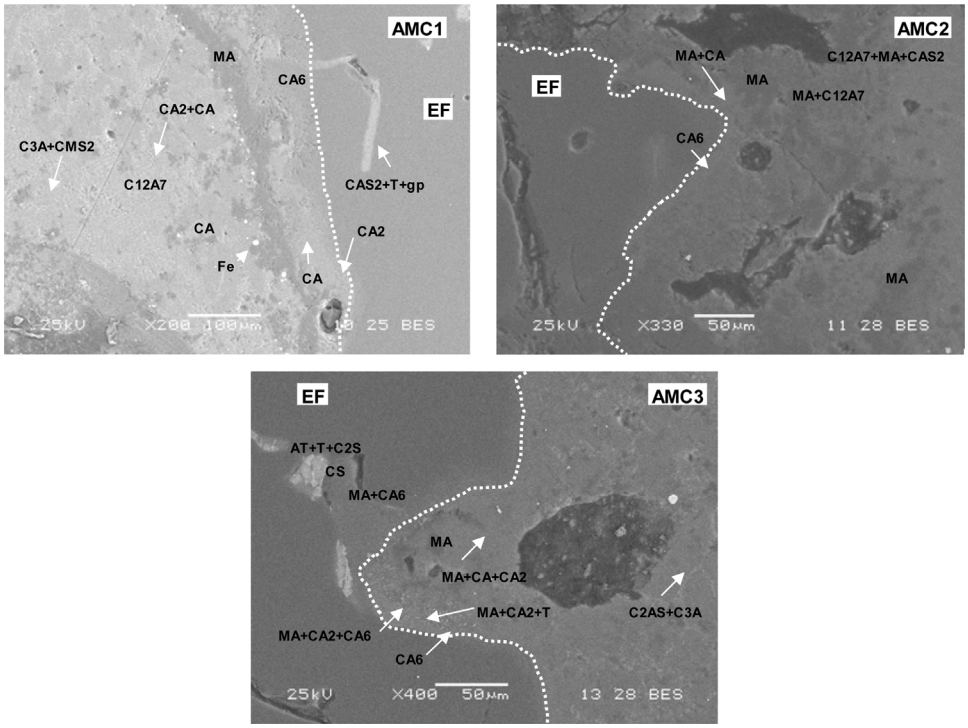

Fig. 11. Brown electrofused alumina aggregates (EF) corroded by the slag (gp: glassy phase). ($C_3A = 3CaO{\cdot}Al_2O_3$, $C_{12}A_7 = 12CaO{\cdot}7Al_2O_3$, $CA = CaO{\cdot}Al_2O_3$, $CA_2 = CaO{\cdot}2Al_2O_3$, $CA_6 = CaO{\cdot}6Al_2O_3$, $C_2S = 2CaO{\cdot}SiO_2$, $CS = CaO{\cdot}SiO_2$, $C_2AS = 2CaO{\cdot}SiO_2{\cdot}Al_2O_3$, $CAS_2 = CaO{\cdot}Al_2O_3{\cdot}2SiO_2$, $CMS_2 = CaO{\cdot}MgO{\cdot}2SiO_2$, $MA = MgO{\cdot}Al_2O_3$, $T = TiO_2$, $AT = Al_2O_3{\cdot}TiO_2$, $Fe = Fe^0$, gp: glassy phase.)

binary phase CS ($CaSiO_3$) was identified in AMC1. This phase involves liquid formation at temperatures higher than 1400 °C.[37] The high SiO_2 concentration close to the aggregates was a consequence of the dissolution of the finest particles in the matrix, being the components with a higher content of silica: bauxite in AMC3 and sintered magnesia in AMC2.

SEM images of the brown electrofused alumina aggregates (EF) of AMC refractories attacked by the slag are shown in Fig. 11 (dotted lines indicate the particle–slag interfaces). Similar characteristics were observed in the three materials with respect to the coarse tabular alumina particles. Furthermore, a high level of Ti was detected in AMC3 (significantly higher than those of AMC1 and AMC2), thus forming Al_2TiO_5 or rutile (TiO_2). This great amount of titanium in AMC3 was attributed to the presence of fine bauxite particles in the matrix that locally increased the content of ions present as impurities in this raw material (Si^{+4}, Ti^{+4} and $Fe^{+2/+3}$, mainly) when they dissolved. The local concentration was favoured by the high viscosity of the melt, which severely reduced the ionic mobility and the homogenization of ion concentrations.

Coarse bauxite particles, only present in AMC3, exhibited a strongly attacked interface with the slag, and infiltration of the liquid through grain boundaries (presence of ions which were absent in the original aggregates) as can be observe in Fig. 12. The same phases identified near corroded tabular alumina and EF particles were basically detected here. However, the CA_6 phase was hardly detected, and the $MgAl_2O_4$ phases did not crystallize as a continuous layer next to the particle. Binary (C_2S) and ternary (C_2AS) Si-containing phases were detected in the immediate region next to the aggregate, to the contrary of what was observed in the corroded tabular and brown electrofused alumina particles. In this sense, the additional contribution of SiO_2 caused by dissolution of coarse bauxite particles was significant.

The high concentration of sodium in the particle–slag interface that formed binary phases with titanium

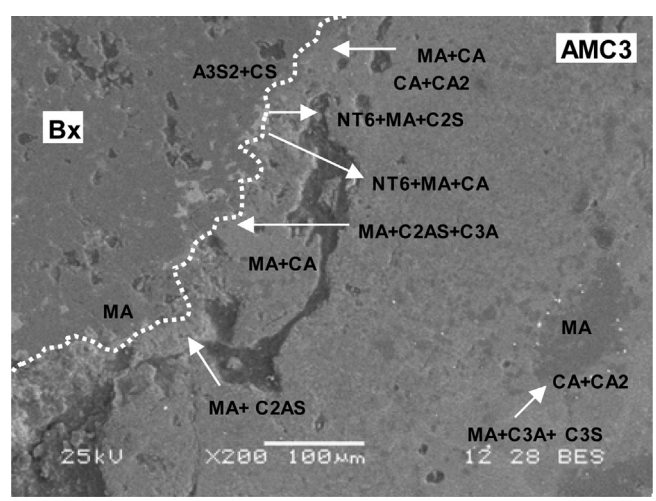

Fig. 12. Bauxite aggregate (Bx) in AMC3 corroded by the slag. ($C_3A = 3CaO{\cdot}Al_2O_3$, $CA = CaO{\cdot}Al_2O_3$, $CA_2 = CaO{\cdot}2Al_2O_3$, $CS = CaO{\cdot}SiO_2$, $C_2S = CaO{\cdot}2SiO_2$, $C_2AS = 2CaO{\cdot}SiO_2{\cdot}Al_2O_3$, $CAS_2 = CaO{\cdot}Al_2O_3{\cdot}2SiO_2$, $M = MgO$, $MA = MgO{\cdot}Al_2O_3$, $A_3S_2 = 3Al_2O_3{\cdot}2SiO_2$, $AT = Al_2O_3{\cdot}TiO_2$, $NT_6 = NaO{\cdot}6TiO_2$.)

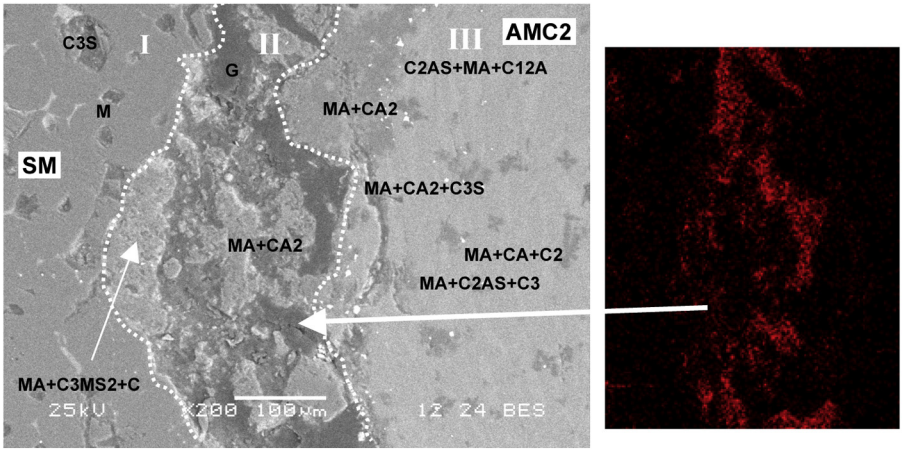

Fig. 13. Sintered magnesia aggregate (SM) in AMC2 corroded by the slag (a) and carbon mapping in the interface region (b). ($C_3A = 3CaO{\cdot}Al_2O_3$, $C_{12}A_7 = 12CaO{\cdot}7Al_2O_3$, $CA = CaO{\cdot}Al_2O_3$, $CA_2 = CaO{\cdot}2Al_2O_3$, $C_3S = 3CaO{\cdot}SiO_2$, $C_2S = 2CaO{\cdot}SiO_2$, $C_3S_2 = 3CaO{\cdot}2SiO_2$, $C_2AS = 2CaO{\cdot}SiO_2{\cdot}Al_2O_3$, $C_3MS_2 = 3CaO{\cdot}MgO{\cdot}2SiO_2$, M = MgO, MA = $MgO{\cdot}Al_2O_3$, G = graphite.)

($NT_6 = NaO{\cdot}6TiO_2$) was striking. As expected, the amount of Ti was also great taking into account the composition of bauxite. The presence of phases with a high proportion of Si around the bauxite, which was glassy in nature ('gp' in Fig. 12), was the result of the additional important contribution of SiO_2 due to dissolution of the superficial layers of the own aggregate and fine particles of the matrix. This was a factor contributing to the low corrosion resistance of this type of particle, as has been pointed out in the literature.[9]

Finally, sintered magnesia aggregates (Fig. 13), which were only present in AMC2 material, showed a severe slag attack through the grain boundaries and direct corrosion[30] with spinel $MgAl_2O_4$ formation; this agrees with observations by other authors.[38] Different zones are distinguished in image (a) of Fig. 13. From the left to the right of the image (Fig. 13a), in the first zone labelled as I, the penetrated aggregate, but without a severe attack, was observed. Beside this zone, an intermediate region II was found where the particle, partially reacted with the slag, formed spinel. The texture of this phase suggested a solid state reaction as the periclase particle came into contact with the Al^{+3} of the melted slag, but without a complete previous dissolution of MgO. The mapping of carbon (Fig. 13b) shows the presence of the pack resin, indicating severe deterioration in this region. Finally, the region III was defined, where phases formed with the ions incorporated into the melt by the complete dissolution of the outer layers of the particle, mainly Mg^{+2}, and Ca^{+2} and Si^{+4} in lower proportions, were identified. The aspect of the spinel detected in this last region suggested that it was formed by precipitation from the liquid,[38] which was saturated in MgO, contrary to that of zone II.

Binary and ternary phases, such as C_3S and merwinite (C_3MS_2), were identified between zones I and II, which suggested the presence of 'inner slag', as has been reported by Wang et al.[38] The ion Si^{4+} was also generated by the dissolution of magnesia particles; binary (C_2S and C_3S) and ternary (C_2AS) phases containing this component were therefore detected in zone III.

The calcium aluminate accompanying spinel was CA_2, while C_3A and $C_{12}A_7$ were detected closer to the slag and which could be phases belonging to the unreacted slag that re-crystallized during cooling (only Ca linked to Al and Si in phases such as gehlenite or anorthite has been reported in literature). Within the slag, spinel was present as small isolated clusters of particles. The spinel crystals' features were consistent with a reduction in the Mg^{+2} concentration as the distance from the sintered magnesia particle increased. The fact that MA spinel had precipitated without continuity envisaged a low inhibition to corrosion by this phase.

3.6. Analysis of the determining factors of corrosion

An approximate thermodynamic analysis of the interaction of AMC refractories with the basic slag used in this study can be performed considering the main components of both systems (refractory and slag): Al_2O_3, CaO and MgO. In Fig. 14, the location of the global compositions of each refractory (black points) and the slag (grey point) within the isothermal section at 1450 °C in the condensed phases equilibrium diagram Al_2O_3–CaO–MgO (FactSage v.6.3.1.) is shown. Compositions corresponding to AMC1 and AMC3 are in equilibrium with the same liquid L_I (grey square). Liquid L_{II} (also identified with a grey square) is in equilibrium with AMC2 at 1450 °C.

Since the composition of the slag is different from those liquids (L_I and L_{II}) in equilibrium with the (simplified) refractory compositions, dissolution of the three AMC materials in contact with this slag is expected, as has been experimentally verified. Because the difference between the composition of L_I and the slag is greater than the difference between L_{II} and the slag, the dissolution of AMC1 and AMC3 would be higher than that of AMC2. On the other hand, once the simplified composition of refractories AMC1 and AMC3 reacts with the slag and shifts in the direction indicated by the arrows in Fig. 14, the compatible phases would be spinel MA, corundum and a liquid with CaO and Al_2O_3 as the major components. For the composition

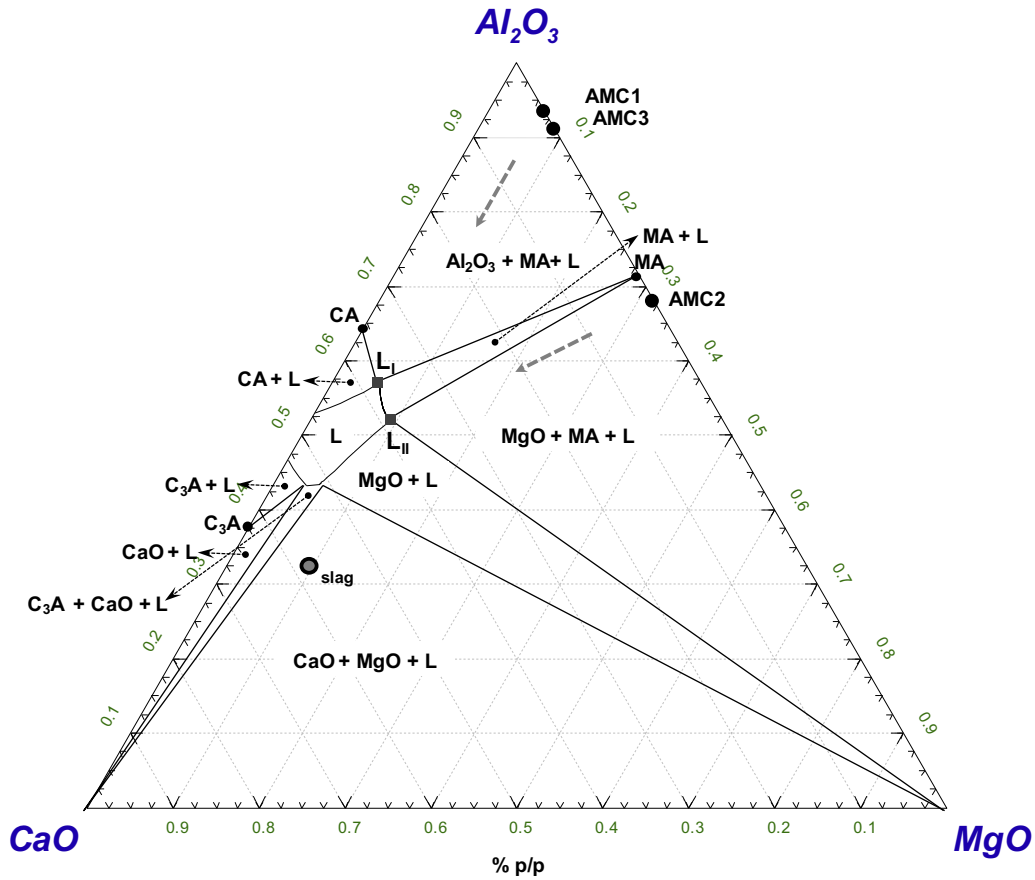

Fig. 14. Isothermal section of Al_2O_3–CaO–MgO equilibrium diagram at 1450 °C.

corresponding to AMC2, the equilibrium phases would be MA spinel, periclase and a liquid similar to the previous one.

Bearing in mind the experimental results that showed AMC2 as undergoing the highest corrosion, it can be asserted that the chemistry of the (global) systems did not determine the differences between the corrosion behaviour of AMC refractories and the basic slag studied here. This demonstrates the importance of minor components and, on the other hand, the effect caused by the local ion concentration at the slag–refractory interface, which strongly depends on the diffusion rate of species (kinetic factor) as well as microstructural and textural effects. None of these factors were considered in the thermodynamic estimation.

However, several of the phases detected in SEM/EDS analyses of the corroded cups (Section 3.2) agreed with the thermodynamic prediction: (a) spinel at the attacked region neighbouring the alumina aggregates, and (b) periclase and spinel around the magnesia particles in AMC2. Regardless, other experimentally identified phases, such as the CA_6, were not equilibrium phases. Calcium hexaluminate was a product of the reaction of lime coming from the melted slag with Al_2O_3, the concentration of which was locally increased by the dissolution of particles containing corundum and the slow diffusion of ions (kinetic factor).

The presence of a continuous layer of $MgAl_2O_4$ spinel in front of the tabular and brown electrofused alumina particles in AMC1, whereas this solid precipitated as an isolated particles in AMC2 and AMC3 since, was another result related to the competition between the kinetic and thermodynamic factors. It evidenced that the local MgO concentration was higher in AMC1, even when AMC2, for example, had the highest nominal content of MgO (∼6 wt.% in AMC1 and ∼27 wt.% p/p in AMC2). According to the study of thermal evolution (Section 1), a greater amount of spinel was formed and/or faster spinelization took place in AMC1 with respect to AMC2 and AMC3. This *in situ* spinel formed in the matrix is usually characterized by a fine granulometry, and the reaction could generate porosity; for these reasons, these particles are expected to dissolve easily into the melt, thus releasing Mg^{+2} and Al^{+3}. Another feature related to these same factors was the higher definition that the CA_6 layer around the tabular alumina particles had, whereas this solid was difficult to detect around bauxite (in AMC3). This difference was attributed to a higher concentration of Al_2O_3 around the TA coarse particles compared with bauxite, because the presence of ions such as Si^{+4}, Ti^{+4} and Fe^{+2}, which came from the dissolution of the matrix, had a dilution effect on Al_2O_3; in consequence, the tendency of calcium hexaluminate to form decreased.

In the case of coarse sintered magnesia particles, the presence of calcium aluminates, which are non-equilibrium solid phases, suggested that the local concentration of Al_2O_3 and CaO

increased, thus favouring its formation. Conversely, it has been reported in literature that Ca is associated with Si and Mg in forming ternary phases, thus indicating that in the present corrosion tests there was less homogenization of the species into the melt (favoured by the absence of stirring).

Since the global chemical composition was discarded as the determining factor behind the corrosion of the AMC refractories and the basic slag evaluated in the present work, other factors have to be considered. Taking into account the composition and microstructure of aggregates composing AMC1, AMC2 and AMC3, it could be considered that susceptibility to the basic slag attack will be higher for sintered magnesia and bauxite particles due to their grain boundaries and secondary phases, which diminish the liquid viscosity,[35] as well as the presence of silicon in both cases, which forms ternary phases with low melting points (such as anorthite and gehlenite). Due to the reduction in the amount of grain boundaries and the increase in grain size, EF aggregates will be more resistant to corrosion, although the presence of Ti could limit this ability.[35] Finally, TA is the type of particle that undergoes little degradation (even the difference with electrofused particles has been questioned[35]).

The higher proportion of tabular alumina in AMC1 would contribute to its higher corrosion resistance with respect to AMC2, which contains the greater amount of sintered magnesia, and AMC3, which is the only refractory formulated with bauxite.

Considering the refractory as a whole, another aspect having a strong influence on the corrosion behaviour is the porosity, in particular, the apparent porosity, the interconnection between pores (or permeability), and the pore sizes. In this sense, the original AMC2 brick has the highest values of open porosity and permeability, and an intermediate pore size. Moreover, according to the experimental data indicated in Fig. 2, the apparent porosity of AMC2 tended to be the highest up to 1400 °C (except after treatment at 1000 °C) and a similar evolution of permeability could be expected, with both factors contributing to the higher degradation exhibited by this refractory with respect to AMC1 and AMC3. At the other extreme, AMC3 has the lowest amount of open pores, of small size, and with permeability significantly lower than that of AMC2 and AMC1. Moreover, the apparent porosity remained below the value reached by the other two materials at 1400 °C. However, even though AMC3 displayed corrosion resistance higher than that of AMC2, this refractory underwent more degradation than AMC1 due to the presence of bauxite, a smaller quantity of tabular alumina and a decreased tendency to undergo spinelization as the temperature increased.

Regarding the content of graphite, unfortunately, the poor state of the bonding phase of corroded cups inhibited the detection of flakes at the refractory–slag interfaces. On the other hand, it was hard to determine the extent of graphite oxidation by atmospheric O_2 or FeO coming from the slag[30] by observing the corroded cup cross sections only. The low amount of iron in the slag composition suggested that its contribution to graphite loss according to the general mechanism of corrosion of oxide–C refractories proposed by Lee and Zhang[30] was very small.

The results of the study with respect to direct oxidation of graphite in air (Section 2) suggested that if the partial loss of graphite occurred during the corrosion tests and rather less at the refractory–slag interface, it was likely that the original order of graphite content, AMC1 < AMC3 < AMC2, would have been inverted. Regardless of whether the graphite was lost in a significant way at the interface region or not, the role of this component was not a determining factor in the difference observed between the AMC refractories. Even so, it is possible that the loss of graphite had some impact on the high susceptibility of AMC2 to the basic slag studied in the present work.

4. Conclusions

From the evaluation of the chemical wear of three commercial AMC refractories at high temperatures against O_2 from air and basic slag, conditions to which the bricks could be exposed during service, variations in their behaviour were, in general, related to the primary differences in their composition, *i.e.*, the content of magnesia and the type of alumina source. These variables directly influence the slag corrosion of AMC refractories. Other microstructural and textural factors, together with their thermal evolution, also affected this behaviour; these were determining factors affecting the susceptibility of AMC refractories to attack by oxygen from air since the process was controlled by diffusion of the gas into the material. In this way, compositional factors indirectly affected resistance to the direct oxidation of graphite through their effect on the packing, the open porosity and the interconnection between pores (permeability).

It was established that the AMC2 refractory, which contains the higher proportion of sintered magnesia in the medium-sized and fine fraction, is the most susceptible to corrosion by both agents. Its lower resistance to air oxidation was determined by the factors that controlled the entrance of oxygen into the material: open porosity, initial permeability and their change as temperature increased up to 1400 °C. They affected the pyrolisis of resin as well as the direct oxidation of graphite. Moreover, the smaller size of the graphite flakes also had an influence on their susceptibility to be oxidized. The same factors contributed to the liquid slag corrosion as well as the high proportion of sintered magnesia particles in AMC2, which are the more reactive components against slag. Although it could be expected that the formation of fine spinel in the matrix is encouraged in AMC2 by its greater amount of MgO, the experimental results showed an opposite tendency, which negatively influenced the response of this refractory against the melted slag.

As for the other two refractories, AMC3 is the material with the highest resistance to air oxidation among the three studied bricks due to its small value of apparent porosity, even when temperature increased, low permeability and pore size, and the higher inherent resistance to oxidation of its own graphite flakes. Meanwhile, AMC1 exhibited the highest liquid corrosion resistance, mainly due to a larger amount of tabular alumina, which is the most chemical resistant particle, and the facility to form fine $MgAl_2O_4$ spinel when temperature rises up.

Acknowledgment

This work was supported by the Agencia Nacional de Promoción Científica y Tecnológica (ANPCyT) of Argentina under the Project "Degradación termoquímica y termomecánica de refractarios óxido-C de uso siderúrgico" (PICT2006N° 1887).

References

1. Koley RK, Rao KAV, Askar S, Srivastava SK. Development and application of Al_2O_3–MgO–C refractory for secondary refining ladle. In: *Proceedings of the Unified International Technical Conference on Refractories UNITECR'01*. 2001.
2. Tassot P, Etienne F, Wang J, Atkinson P. New concepts for steel ladle linings. In: *Proceedings of the Unified International Technical Conference on Refractories UNITECR'07*. 2007. p. 462–5.
3. Chatterjee S, Eswaran R. Optimization of slag corrosion resistance and thermal expansion in Al_2O_3–MgO–C brick. In: *Proceedings of the Unified International Technical Conference on Refractories UNITECR'09*. 2009.
4. Sasajima Y, Yoshida T, Hayama S. Effect of composition and magnesia particle size in alumina–magnesia–carbon refractories. In: *Proceedings of the Unified International Technical Conference on Refractories UNITECR'89*. 1989. p. 586–603.
5. Watanabe A, Takahashi H, Takanaga S, Goto N, Matsuura O, Yoshida S. Thermal and mechanical properties of Al_2O_3–MgO–C bricks. *Taikabutsu Overseas* 1990;**10**(3):137–47.
6. Gupta AD, Vickram K. Development of resin-bonded alumina–magnesia–carbon bricks for steel ladle applications. *Interceram* 1999;**48**(5):307–10.
7. Kamiide M, Yamamoto S, Yamamoto K, Nakahara K, Kido N. Damage of Al_2O_3–MgO–C brick for ladle furnace. *J Tech Assoc Refract Jpn* 2001;**21**(4):252–7.
8. Resende WS, Stoll RM, Justus SM, Andrade RM, Longo E, Baldo JB, et al. Key features of alumina/magnesia/graphite refractories for steel ladle lining. *J Eur Ceram Soc* 2000;**20**:1419–27.
9. Pötschke J, Deinet T, Routschka G, Simmat R. Properties and corrosion of AMC-refractories. Part II: corrosion by steel/slag. In: *Proceedings of the Unified International Technical Conference on Refractories UNITECR'03*. 2003. p. 584–7.
10. Camerucci MA, Galliano PG, Cavalieri AL, Tomba Martinez AG. Chemical wear of commercial magnesia–carbon refractories bricks in air. *Interceram* 2012;**61**(4):198–204.
11. Muñoz V, Pena P, Tomba Martinez AG. Physical, chemical and thermal characterization of Al_2O_3–MgO–C refractories. *Ceram Int* 2014;**40**:9133–49.
12. Browning GJ, Bryant GW, Hurst HJ, Lucas JA, Wall TF. An empirical method for the prediction of coal ash slag viscosity. *Energy Fuels* 2003;**17**(3):731–7.
13. Muñoz V, Tomba Martinez AG. Thermal evolution of Al_2O_3–MgO–C refractories. *Procedia Mater Sci* 2012;**1**:410–7.
14. Baudín C, Álvarez C, Moore RE. Influence of chemical reactions in magnesia–graphite refractories I. Effects on texture and high temperature mechanical properties. *J Am Ceram Soc* 1999;**82**(12):3529–38.
15. Rand B, McEnaney B. Carbon binder from polymeric resins and pitch, Part I – pyrolysis behaviour and structure of the carbons. *Br Ceram Trans J* 1985;**84**(5):157–65.
16. Gardziella A, Suren J, Belsue M. Carbon form phenolic resins: carbon yield and volatile components – recent studies. *Interceram* 1992;**41**(7/8):461–7.
17. Costa L, Rossi di Montelera L, Camino G, Weil ED, Pearce EM. Structure-charring relationship in phenol-formaldehyde type resins. *Polym Degrad Stab* 1997;**56**:23–35.
18. Kapteijn F, Meijer R, Moulijn JA, Cazorla-Amorós D. On why do different carbons show different gasification rates: a transient isotopic CO_2 gasification study. *Carbon* 1994;**32**(7):1223–31.
19. Moulijn JA, Kapteijn F. Towards a unified theory of reactions of carbon with oxygen-containing molecules of carbon. *Carbon* 1995;**33**(8):1155–65.
20. McKee DW. Metal oxides as catalysts for the oxidation of graphite. *Carbon* 1970;**8**(8):623–35.
21. Jiang W, Nadeau G, Zaghib K, Kinoshita K. Thermal analysis of the oxidation of natural graphite – effect of particle size. *Thermochim Acta* 2000;**351**:85–93.
22. Xiaowei L, Jean-Charles R, Suyuan Y. Effect of temperature on graphite oxidation behaviour. *Nucl Eng Des* 2004;**227**:273–80.
23. Doughty GR, Tovey LS. A comparison of the oxidation behaviour in air at 1050 °C of natural flake graphites. In: *Proceedings of the Unified International Technical Conference on Refractories UNITECR'93*. 1993. p. 831–9.
24. Li X, Rigaud M, Palco SJ. Oxidation kinetics of graphite phase in MgO–C refractories. *J Am Ceram Soc* 1995;**78**(4):965–71.
25. Takeuchi K, Yoshida S, Tsuboi S. Gas phase oxidation of MgO–C bricks. *J Tech Assoc Refract Jpn* 2003;**23**(4):276–9.
26. Sadrnezhaad SK, Mahshid S, Hasemi B, Nemati ZA. Oxidation mechanism of C in MgO–C refractory bricks. *J Am Ceram Soc* 2006;**89**(4):1308–16.
27. Pötschke J, Deinet T, Routschka G, Simmat R. Properties and corrosion of AMC-refractories. Part I: characterisation and oxidation. In: *Proceedings of the Unified International Technical Conference on Refractories UNITECR'03*. 2003. p. 580–3.
28. Özgen OS, Rand B. Kinetics of oxidation of the graphite phase in alumina/graphite materials II – materials with different graphite content, graphite flake size and with clay or carbon bonds. *Br Ceram Trans J* 1985;**84**:213–8.
29. Ko T, Kuo W, Chang Y. Microstructural changes of phenolic resin during pirolisis. *J Appl Polym Sci* 2001;**81**:1084–9.
30. Lee WE, Zhang S. Melt corrosion of oxide and oxide–carbon refractories. *Int Mater Rev* 1999;**44**(3):77–104.
31. Bradaschia C. *Siderurgia para não siderurgistas*. Associação Brasileira de Metalurgia, Materiais e Mineração; 1986.
32. Lee WE, Zhang S, Marriott NJ, Sarpoolaky H. Influence of microstructure on refractories corrosion. In: *Proceedings of the Unified International Technical Conference on Refractories UNITECR'01*. 2001. p. 2–10.
33. Shi C. Steel slag-its production, processing, characteristics, and cementitious properties. *J Mater Civ Eng* 2004;(May/June):230–6.
34. Waligora J, Bulteel D, Degrugilliers P, Damidot D, Potdevin JL, Meassond M. Chemical and mineralogical characterizations of LD converter steel slags: a multi-analytical techniques approach. *Mater Charact* 2010;**61**:39–48.
35. Sarpoolaky H, Zhang S, Argent BB, Lee WE. Influence of grain phase on slag corrosion of low-cement castable refractories. *J Am Ceram Soc* 2001;**84**(2):426–34.
36. Sandhage KH, Yurek GJ. Indirect dissolution of sapphire into silicate melts. *J Am Ceram Soc* 1988;**71**(6):478–89.
37. Verein Deutsher Eisenhittenleute (VDEh), editor. *Slag Atlas*. 2nd ed. D.Düsseldorf: Verlag StahLeisen GmbH; 1995.
38. Wang D, Li X, Wang H, Mi Y, Jiang M, Zhang Y. Dissolution rate and mechanism of solid MgO particles in synthetic ladle slags. *J Non-Cryst Solids* 2012;**358**:1196–201.